minerals

MDPI

Article

X-ray and Neutron Study on the Structure of Hydrous SiO_2 Glass up to 10 GPa

Satoru Urakawa [1,*], Toru Inoue [2,3], Takanori Hattori [4], Asami Sano-Furukawa [4], Shinji Kohara [5,6], Daisuke Wakabayashi [7], Tomoko Sato [2], Nobumasa Funamori [7] and Ken-ichi Funakoshi [8]

1 Department of Earth Sciences, Okayama University, Okayama 700-8530, Japan
2 Department of Earth and Planetary Systems Science, Hiroshima University, Higashi-Hiroshima 739-8526, Japan; toinoue@hiroshima-u.ac.jp (T.I.); tomokos@hiroshima-u.ac.jp (T.S.)
3 Geodynamics Research Center, Ehime University, Matsuyama 790-8577, Japan
4 J-PARC Center, Japan Atomic Energy Agency, Tokai 319-1195, Japan; hattori.takanori@jaea.go.jp (T.H.); sanoasa@post.j-parc.jp (A.S.-F.)
5 Research Center for Advanced Measurement and Characterization, National Institute for Materials Science (NIMS), Sayo, Hyogo 679-5148, Japan; KOHARA.Shinji@nims.go.jp
6 Diffraction and Scattering Division, Japan Synchrotron Radiation Research Institute, Sayo, Hyogo 679-5198, Japan
7 Institute of Materials Structure Science, High Energy Accelerator Research Organization (KEK), Tsukuba 305-0801, Japan; daisuke.wakabayashi@kek.jp (D.W.); nobumasa.funamori@kek.jp (N.F.)
8 Neutron Science and Technology Center, Comprehensive Research Organization for Science and Society, Tokai 319-1106, Japan; k_funakoshi@cross.or.jp
* Correspondence: urakawa@okayama-u.ac.jp

Received: 15 December 2019; Accepted: 16 January 2020; Published: 20 January 2020

Abstract: The structure of hydrous amorphous SiO_2 is fundamental in order to investigate the effects of water on the physicochemical properties of oxide glasses and magma. The hydrous SiO_2 glass with 13 wt.% D_2O was synthesized under high-pressure and high-temperature conditions and its structure was investigated by small angle X-ray scattering, X-ray diffraction, and neutron diffraction experiments at pressures of up to 10 GPa and room temperature. This hydrous glass is separated into two phases: a major phase rich in SiO_2 and a minor phase rich in D_2O molecules distributed as small domains with dimensions of less than 100 Å. Medium-range order of the hydrous glass shrinks compared to the anhydrous SiO_2 glass by disruption of SiO_4 linkage due to the formation of Si–OD deuterioxyl, while the response of its structure to pressure is almost the same as that of the anhydrous SiO_2 glass. Most of D_2O molecules are in the small domains and hardly penetrate into the void space in the ring consisting of SiO_4 tetrahedra.

Keywords: hydrous silica glass; medium-range order; first sharp diffraction peak; phase separation; small angle X-ray scattering; X-ray diffraction; neutron diffraction; high pressure

1. Introduction

Silica glass is the most fundamental, fully polymerized network glass whose structure and properties under pressure have long been of interest as an important analog material of silicate magma [1–9]. For the structural aspect, SiO_2 glass is densified by compression with the change in medium-range order in the pressure region up to about 10 GPa [2,4,8]. Namely, reduction of the Si–O–Si bond angle between SiO_4 tetrahedra shrinks the ring and squeezes the interstitial void, leading to permanent densification of SiO_2 glass. SiO_2 glass becomes fully densified glass by room temperature compression to the pressure of 9 to 13 GPa, of which the density is about 20% higher than ordinary SiO_2 glass at ambient conditions [8].

Water in silicate glass has a large effect on the structure as well as on the properties such as viscosity and glass transition temperature [10,11]. Water can react with SiO_2 glass to form hydroxyl species (Si–OH), disrupting the linkage of SiO_4 tetrahedra. As a result, the medium-range order of the SiO_2 glass is also affected by the addition of water in which the size of the ring of the SiO_2 glass containing water becomes smaller than that of ordinary SiO_2 glass [12]. The molecular water, as well as the hydroxyl, is also present in the silicate glasses. It is known that the molecular water becomes the dominant water species in the silicate glasses with increasing total water content [10,11]. However, it is not yet well understood how the molecular water is incorporated into the silicate glasses.

In this study, the hydrous SiO_2 glass containing 13 wt.% of D_2O was synthesized under high-pressure and high-temperature conditions and small angle X-ray scattering (SAXS), X-ray diffraction (XRD), and neutron diffraction (ND) have been applied in order to investigate the short-range order, medium-range order, and phase separation of this hydrous glass. In addition to this, in-situ high-pressure XRD and ND measurements of this hydrous glass have been conducted up to about 10 GPa to clarify the pressure response of its structure. Effects of the pressure and the water dissolution on the medium-range order of the SiO_2 glass and the state of molecular water in the SiO_2 glass are also discussed.

2. Hydrous SiO_2 Glass Sample

The glass sample with a composition of SiO_2–13wt.% D_2O was synthesized using a Kawai-type high-pressure apparatus driven by the 3000 ton press installed at GRC, Ehime University. Powdered quartz enclosed in a Pt capsule together with 13 wt.% D_2O was melted at 3 GPa and 1873 K for 30 min, then it was quenched to room temperature by turning off the electric power supply. The quenching rate was approximately 1000 K/s. Subsequently, the applied pressure was released slowly in several hours, and then the sample was recovered in ambient conditions (Figures S1 and S2). Since we have not measured the content of heavy water in SiO_2 glass, the 13 wt.% D_2O content is a nominal value. The recovered glass is optically clear and homogeneous. Density of this hydrous SiO_2 glass was determined to be 2.239 g/cm^3 by Archimedes' method. This value is slightly higher than the density of ordinary SiO_2 glass (2.20 g/cm^3), although it contains a large amount of heavy water. This means that this high-pressure hydrous SiO_2 glass is an intermediately densified glass.

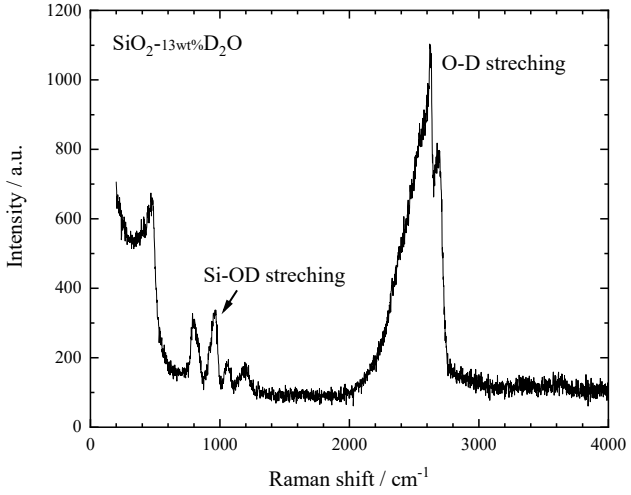

Figure 1. Raman spectrum of the hydrous SiO_2 glass at ambient conditions. Spectrum is unpolarized.

Raman spectroscopy analysis has been applied to clarify the species of water dissolved in the SiO_2 glass. Raman spectrum shows that the hydrous SiO_2 glass has some additional peaks except those assigned to silica glass (Figure 1). Those are a sharp peak around 960 cm^{-1} and a broad peak from 2100 to 2750 cm^{-1}. The former is assigned to the Si–OD stretching vibrations and the latter to OD

stretching vibrations in D_2O molecules and Si–OD groups [13,14]. Heavy water in the hydrous SiO_2 glass is thought to take two states, OD deuterioxyl and D_2O molecule. In general, the amount of OH hydroxyls dissolved in the silicate glass increases with the total H_2O content, but reaches a limit of about 3 wt.% [10,11]. Thus, this hydrous SiO_2 glass may contain about 10 wt.% of the heavy water as molecular species.

3. Experiments

3.1. Small Angle X-ray Scattering at Ambient Conditions

SAXS experiments were performed at the BL18C of the Photon Factory (PF) of the High Energy Accelerator Research Organization (KEK), Japan. Incident X-rays were monochromatic X-rays of 15.28 keV with a beam diameter of 35 micrometers, and scattered X-rays were detected in Q-range from 0.02 to 4.0 $Å^{-1}$ with an image plate. The detail of experimental setup is described elsewhere [15].

3.2. Angle-Dispersive X-ray Diffraction at Ambient Conditions

Angle-dispersive XRD experiment at ambient conditions was carried out using two-axis diffractometer at the BL04B2 beamline of SPring-8, Japan. We acquired diffraction data up to Q = 25 $Å^{-1}$ by angle dispersive method using the monochromatic X-rays of 61.37 keV. The detail of the experimental setup is described elsewhere [16,17].

3.3. High-Pressure X-ray Diffraction

XRD experiments on the hydrous glass during compression were performed using the DIA-type cubic press MAX80 installed at the AR-NE5C beamline of the PF. Tungsten carbide anvils and a boron-epoxy pressure transmitting medium were used. A powdered sample was pressed into a pellet with a diameter of 2 mm and enclosed in a boron nitride (BN) capsule. Sample pressure was determined from the volume of the NaCl pressure marker [18]. XRD profiles were acquired by an energy-dispersive method in a transmitting geometry with an intrinsic Ge detector at room temperature and pressures of up to 9.6 GPa. White X-rays up to 120 keV were used and the data was collected at 11 fixed angles ranging from 3° to 30° to cover a wide Q range. Background intensities were also measured at each angle using an empty cell.

3.4. High-Pressure Neutron Diffraction

ND experiments of the hydrous SiO_2 glass under pressure were conducted by the time-of-flight (TOF) method combined with a multi-anvil press ATSUHIME [19] at the PLANET beamline [20] of the spallation neutron source of the Materials and Life Science Experimental Facility (MLF) at the J-PARC, Japan. A multi-anvil 6-6 type high-pressure apparatus was used [21]. The second-stage Ni-bound WC anvils were used. Clumps of SiO_2–13wt.%D_2O glasses were directly packed in the ZrO_2 pressure medium. The size of the hydrous SiO_2 glass sample was 4.7 mm in diameter and 6.7 mm in height. Sample pressures were calculated on the basis of the pressure-load calibration curves which were determined in separated runs beforehand. The diffracted neutrons were detected by a pair of 90° detector banks consisting of ^{3}He position sensitive detectors equipped with receiving radial collimators. The data were acquired for 15–33 h at the proton beam power of 300 kW. ND profiles were acquired at room temperature and with the same pressure conditions as those of XRD experiments. Diffraction profiles of a vanadium pellet in a high-pressure cell and an empty cell were also acquired for the correction of scattering intensity.

4. Results and Discussion

4.1. Phase Separation of Hydrous SiO_2 Glass

It is known that the silicate glass with high water content undergoes the glass-in-glass phase separation at a low temperature [11]. Due to the limitation of mutual solubility, it separates into a

silica-rich and a water-rich phase. We performed the SAXS measurements on several parts of the hydrous SiO_2 glass to clarify the possible phase separation. The hydrous SiO_2 glass clearly shows significant scattering intensity compared with anhydrous glass (Figure 2). The scattering intensity, however, shows a difference depending on location; some regions have strong scattering intensity, while others only show very weak scattering intensity. This indicates that the distribution of scattering entities in the hydrous glass is heterogeneous in the dimension on the order of from μm to mm. The SAXS patterns of the hydrous glass has a broad peak at Q = 0.05–0.1 Å^{-1}, which indicates the existence of an average distance frequently realized between neighboring scattering entities. The average distance is estimated to be about 100 Å from the length scale ($2\pi/Q$) corresponding to the position of the peaks. It is, therefore, considered that the size of the scattering entities is less than 100 Å. The similar SAXS pattern was observed in hydrated Na-silicate glass, and it was interpreted by the glass-in-glass phase separation [11]. In our hydrous SiO_2 glass, similar phase separation may occur. When combined with the results of the XRD and ND described below, the most likely candidate for this scattering entities in hydrous SiO_2 glass is a phase rich in molecular D_2O. Although this hydrous glass is optically homogeneous, it is considered to be the mixture of SiO_2-rich glass part and D_2O-rich domain with the dimensions of less than 100 Å.

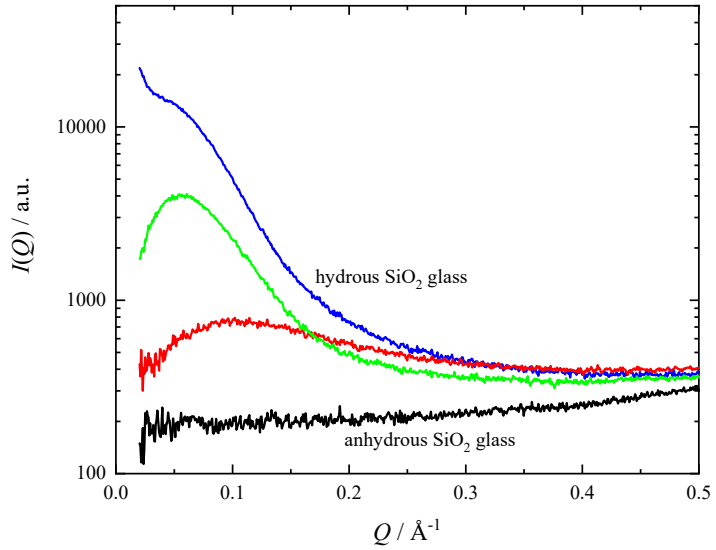

Figure 2. Small angle X-ray scattering intensity from the hydrous SiO_2 glass at ambient conditions. Scattering intensity from anhydrous SiO_2 glass (black curve) is also shown for comparison. Three curves were observed at locations from a few hundred micrometers to a millimeter apart.

4.2. Comparison with Dry SiO_2 Glass at Ambient Conditions

We compare the structure of the hydrous glass and the anhydrous glass at atmospheric pressure using the results of XRD and ND. The structure factors $S(Q)$ and the total correlation functions $T(r)$ for the hydrous and the anhydrous glass are shown in Figure 3. The $S(Q)$ and $T(r)$ for the anhydrous SiO_2 glass were reported by Kohara et al. [22] for X-ray and Hannon [23] for neutron. Here, we consider what the $S(Q)$ and the $T(r)$ of the hydrous SiO_2 glass represent. XRD and ND measurements were performed on the bulk hydrous SiO_2 glass. As shown in the results of the SAXS measurements, the hydrous glass is separated into two phases. Therefore, the $S(Q)$ and $T(r)$ obtained from XRD and ND are the sum of contributions from the SiO_2-rich glass part and the D_2O-rich domains. Hereafter, we discuss the structure of the hydrous SiO_2 glass based on this view.

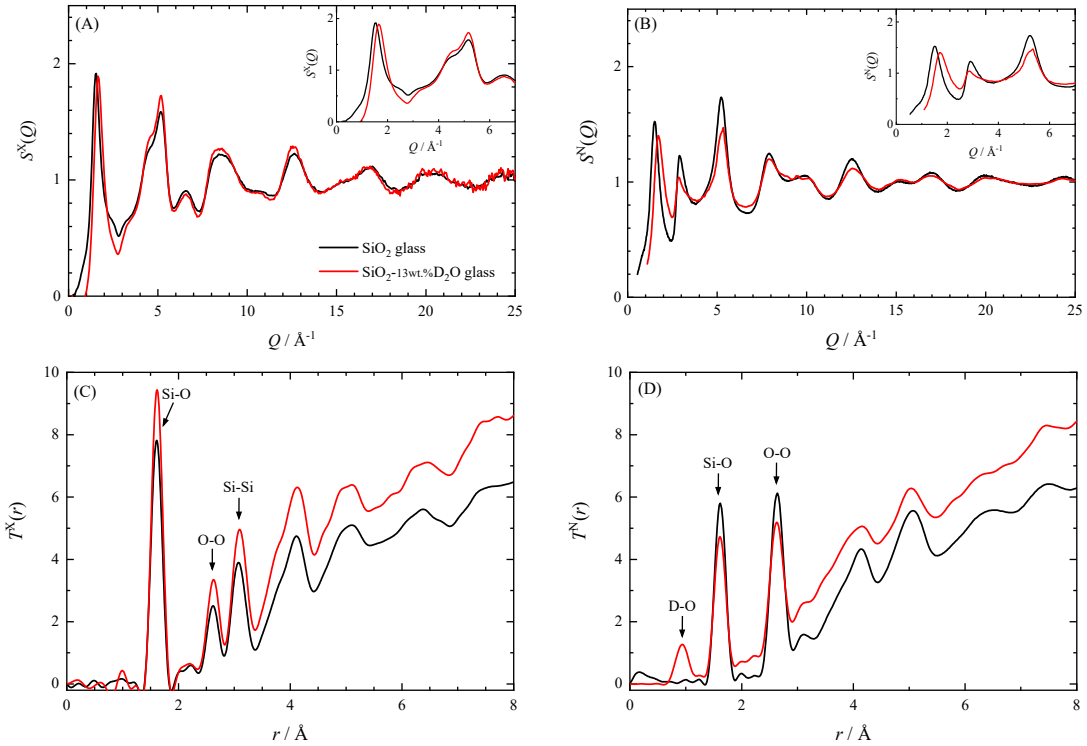

Figure 3. X-ray and neutron diffraction data of the hydrous SiO_2 glass and the anhydrous SiO_2 glass at ambient conditions. (**A**) The X-ray structure factor $S^X(Q)$, (**B**) the neutron structure factor $S^N(Q)$, (**C**) the X-ray total correlation function $T^X(r)$, and (**D**) the neutron total correlation function $T^N(r)$.

As discussed below, both $S(Q)$ and $T(r)$ show that the short-range order composed of SiO_4 tetrahedra of the hydrous SiO_2 glass is almost the same as that of anhydrous glass, while the medium-range order related to the ring of the SiO_4 tetrahedra is diminished by addition of water. The first sharp diffraction peak (FSDP) observed at $Q \sim 1.5$–1.7 Å^{-1} in both the $S^X(Q)$and $S^N(Q)$ of hydrous glass clearly shifts to the higher-Q side than those of anhydrous glass. The second peak is observed at $Q = 2.9$ Å^{-1} only in neutron data. In the other peaks, the intensity and the position of $S^X(Q)$ are almost the same between the hydrous and the anhydrous glass, whereas the $S^N(Q)$ shows a difference. This is due to the very small X-ray atomic scattering factor of D and the relatively large neutron scattering length of D. The similarity of $S^X(Q)$ means the Si–O correlation between the hydrous and anhydrous glass is similar. The X-ray total correlation function $T^X(r)$ of hydrous glass shows almost the same peaks positions as those of anhydrous glass, but the height of $T^X(r)$ of hydrous glass is higher than that of anhydrous glass because of its higher number density. The Si coordination number of the hydrous glass calculated from the area of the first peak at 1.6 Å is about 3.9, which is almost the same as that for the anhydrous glass. On the other hand, the neutron total correlation function $T^N(r)$ of hydrous glass has a different shape from that of anhydrous glass because of the presence of peaks due to the OD deuterioxyl and the D_2O molecules. The peak at about 0.93 Å for hydrous glass corresponds to the D–O distance. In the $T^N(r)$, it is difficult to identify peaks originating from deuterium other than this peak, but the effect of overlapping peaks is recognized. Since the Si-O correlation typically located around 1.6 Å in the $T^N(r)$ is superimposed on the intramolecular D–D correlation (1.56 Å) and the intermolecular O–D correlation (1.92 Å) of D_2O [24], the coordination number of Si cannot be determined.

FSDP of $S(Q)$ is thought to be related to the formation of medium-range order, although its origin has been still under debate [25–29]. The position of FSDP, Q_1, corresponds to the length scale of periodicity in real space l_1 ($=2\pi/Q_1$). Thus, the shift of the FSDP toward high-Q side by dissolution of water means the shrinkage of the medium-range order. This is attributed to the decrease of the

size of the SiO_4 ring by breaking SiO_4 linkages with the OH (OD) group. In ordinary SiO_2 glass, the six-membered ring of SiO_4 tetrahedra is most frequent followed by the five-membered ring [30], but the population of a smaller ring, such as five- and four-membered rings, may increase by water dissolution. The shift of the FSDP toward high-Q side due to water dissolution has been reported for rhyolitic glasses containing more than 70 wt.% of SiO_2 [31]. The displacement of the FSDP of $S^X(Q)$ in rhyolitic glass is about 1.5 $Å^{-1}$ by the 7.5 wt.% dissolution of H_2O, which is comparable to that of our hydrous silica glass containing 13 wt.% of D_2O.

On the other hand, the FSDP of densified SiO_2 glasses is known to be on the high-Q side compared to ordinary SiO_2 glass [32]. This is considered to correspond to the shrinkage of the medium-range order, which is related to a reduction of Si–O–Si bond angle associated with the reduction of interstitial voids by compression [4]. Our hydrous SiO_2 glass was prepared by quenching from the melt at 3 GPa and is thought to partially retain the structure of intermediately densified glass. Therefore, the position of FSDP in our hydrous glass can be attributed to the effects of both water addition and densification.

As revealed by SAXS, XRD, and ND, the hydrous glass synthesized in this study is a mixture of SiO_2-rich glass parts and a D_2O-rich domain. By assuming that the structure of each phase is the same as that for pure SiO_2 glass and pure liquid D_2O, the $S(Q)$ for hydrous glass can be calculated from those for pure phases [22,33–35] (the detailed method is described in Appendix B). Comparison of the $S^X(Q)$ and the $S^N(Q)$ of the hydrous SiO_2 with those calculated from the previously reported $S(Q)$ are shown in Figure 4. They showed good agreement except the position of FSDP of the $S^X(Q)$ and the $S^N(Q)$, and the height of the second peak of the $S^N(Q)$. The difference may be attributed to the shrinkage of the medium-range order of the SiO_2 glass by dissolution of water.

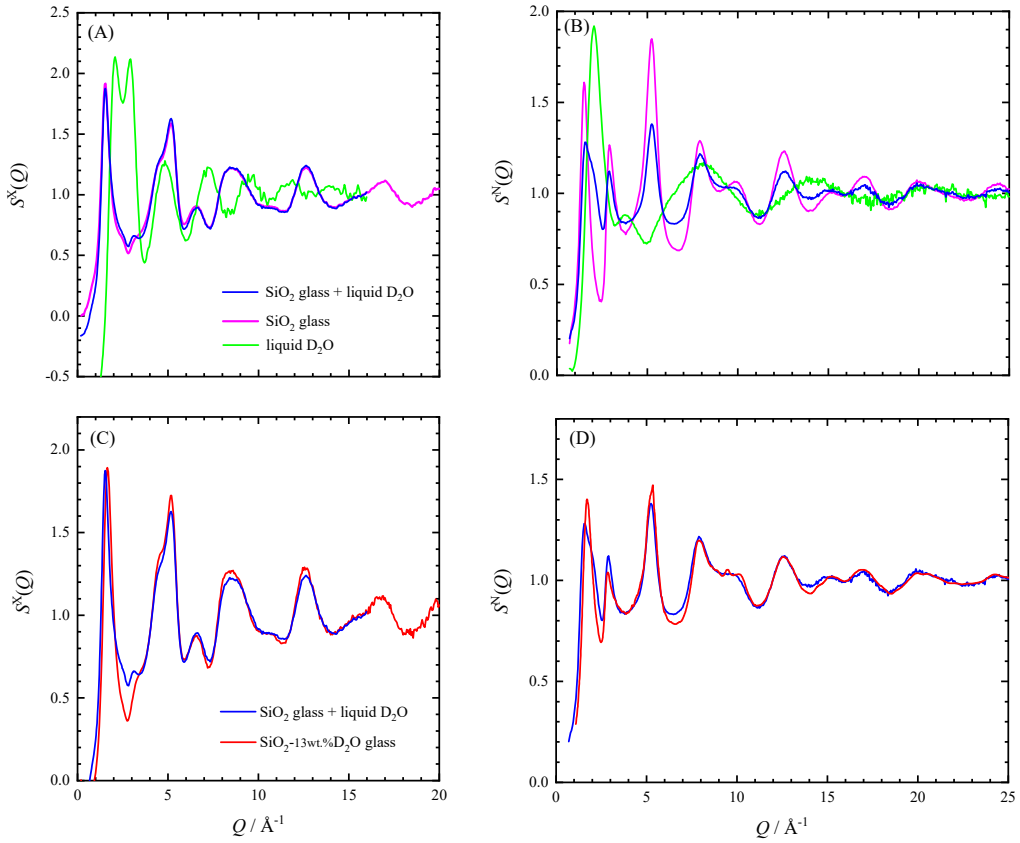

Figure 4. (**A**) $S^X(Q)$'s of SiO_2 glass and liquid D_2O at ambient conditions [22,34], and that simulated for the hydrous glass using them. (**B**) Corresponding $S(Q)$ for neutron, $S^N(Q)$ [33,35]. (**C**) Comparison of the observed and simulated $S^X(Q)$s for the hydrous SiO_2 glass. (**D**) Comparison of the observed and simulated $S^N(Q)$s.

4.3. Hydrous SiO_2 Glass under Pressure

We consider the response of the structure of the hydrous SiO_2 glass to pressure. The $S(Q)$ and $T(r)$ for the hydrous glass during compression to about 10 GPa are shown in Figure 5. In XRD, the $S^X(Q)$ of hydrous SiO_2 glass changes with pressure in the same way as anhydrous SiO_2 glass reported by Inamura et al. [4], except for the position of the FSDP. This means that the response to the pressure of the short-range order of the hydrous glass is the same as that of the anhydrous glass. This is consistent with the structure deduced from SAXS showing that the hydrous SiO_2 glass is mainly composed of relatively dry parts rich in SiO_2.

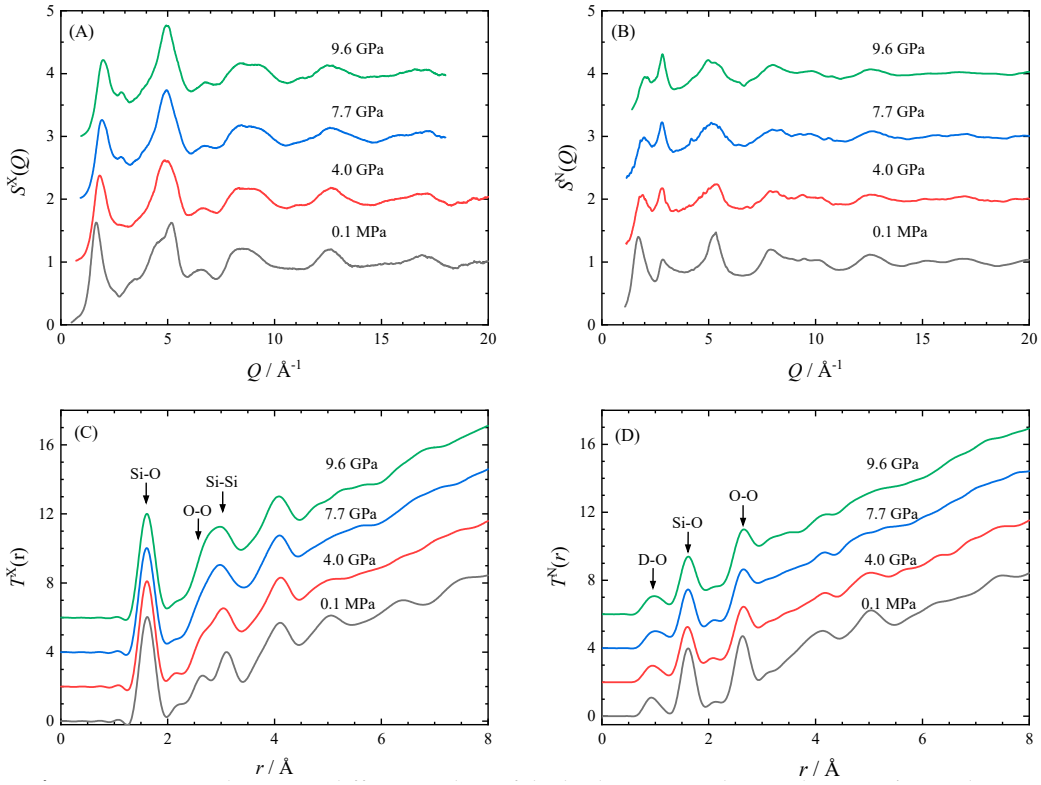

Figure 5. X-ray and neutron diffraction data of the hydrous SiO_2 glass with 13 wt.% D_2O during room temperature compression to 10 GPa. (**A**) The X-ray structure factor $S^X(Q)$, (**B**) the neutron structure factor $S^N(Q)$, (**C**) the X-ray total correlation function $T^X(r)$, and (**D**) the neutron total correlation function $T^N(r)$.

Figure 6 compares the pressure dependence of the position of FSDP of hydrous SiO_2 glass obtained from both XRD and ND with that of anhydrous glass [4,9]. The FSDP of $S^X(Q)$ and $S^N(Q)$ shifts in parallel to the high-Q side in proportion to the pressure up to 10 GPa. Those shifts are also parallel to the FSDP of ordinary anhydrous glass. In addition, the intensity of the FSDP of the hydrous glass decreases with pressure in the same way as anhydrous glass for both the $S^X(Q)$ and $S^N(Q)$ [4,9]. Shrinkage of the medium-range order is also found in $T(r)$. The Si–O distance is almost constant with up to 10 GPa, but the Si–Si distance decreases with increasing pressure (Figure 5). Thus, the Si–O–Si bond angle decreases, and the network linkage of the SiO_4 tetrahedra is distorted with increasing pressure. These show that even though the medium-range order of the hydrous SiO_2 glass is partly disrupted by OD deuterioxyl, it shrinks with pressure just like the anhydrous glass.

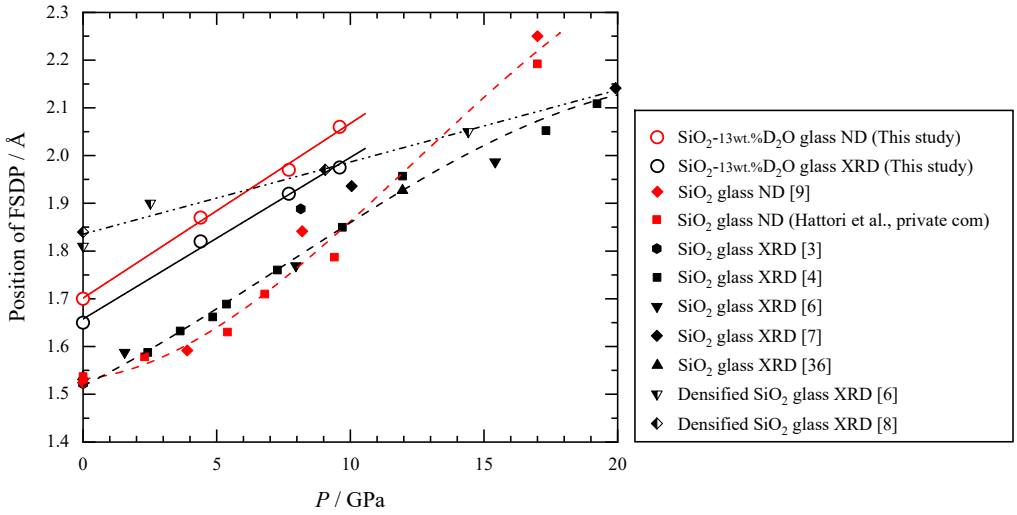

Figure 6. Comparison of the position of the first sharp diffraction peak (FSDP) of $S^X(Q)$ and $S^N(Q)$ between the hydrous and anhydrous SiO_2 glass [3,4,6–8,36].

We estimate the density of hydrous SiO_2 glass under pressure in order to derive the total correlation function $T(r)$. Since the FSDP of the hydrous glass changes with pressure at almost the same rate as that of the anhydrous glass, and the shape of the structure factors resemble each other except the FSDP, we assume that the densities of hydrous glass and anhydrous glass would change in the same rate with pressure. We evaluate the $T(r)$ using the densities of hydrous glass at high pressures, which is estimated from the relationships between density and pressure of ordinary SiO_2 glass shown in Figure 1 of Wakabayashi et al. [8]. The coordination number of Si calculated from $T^X(r)$ is about four up to 10 GPa, which is consistent with that of anhydrous SiO_2 glass. This shows that our estimation of high-pressure density of hydrous SiO_2 glass is fairly good, because the similarity of the short-range order between hydrous glass and anhydrous glass is expected.

What happens to the D_2O-rich phase in the hydrous SiO_2 glass during compression? Unfortunately, neutron diffraction data does not give us any information except nearly constant D–O distance in $T^N(r)$ up to 10 GPa. When evaluated using the partial molar volume of H_2O at 3 GPa [37], at which the hydrous SiO_2 glass was synthesized, 10 wt.% D_2O is equivalent to about 14% in volume. It is interesting that such an amount of molecular D_2O does not greatly affect the compression behavior of SiO_2 glass.

4.4. Molecular Water in the Hydrous SiO_2 Glass

The SAXS strongly suggests that most of the D_2O molecules may form the separate phase in small domains distributed in the hydrous SiO_2 glass. Can all D_2O molecules in the hydrous glass be incorporated into the small domains? Here, we consider the possibility that D_2O molecules are contained in the voids characteristic of the ring structure made by connecting SiO_4 tetrahedra.

Sato et al. [38] showed that when He penetrates into SiO_2 glass, SiO_2 glass becomes rigid. Since the interstitial voids in the SiO_2 glass are occupied by He, the voids are not squeezed even when pressure is applied and the bulk modulus of the SiO_2 glass with He becomes larger than that of the ordinary SiO_2 glass. It is shown that the FSDP position of the SiO_2 glass saturated with He does not change up to 10 GPa. If D_2O molecules penetrate the interstitial voids formed by the SiO_4 linkage, the bulk modulus of the hydrous glass should be larger than that of ordinary glass, as shown in the case of SiO_2 glass with He. The position of the FSDP of our hydrous glass, however, changes with pressure in the same way as the anhydrous glass (Figure 6), and its bulk modulus is estimated to be almost the same as that of the anhydrous glass. Thus, it is considered that the interstitial void space in the hydrous SiO_2 glass is almost empty, and D_2O does not penetrate into the SiO_4 network. It is supported from void size: The interstitial void in the SiO_4 network of SiO_2 glass is too small to accommodate

D_2O molecule in it. In the size distribution model of interstitial voids in silica glass estimated from the solubility site density of He and Ne dissolved in cristobalite, about 10% of voids can contain He and only 6% of voids can contain Ne [39]. According to Zhang and Xu [40], the molecular diameter of H_2O is 2.74 Å (that of D_2O is also expected to be about the same), which is larger than He (2.16 Å) and Ne (2.42 Å), so that it seems difficult to incorporate the H_2O (or D_2O) molecules in the interstitial voids of SiO_2 glass. Further, the void size in the hydrous glass is smaller than that of anhydrous glass due to the reduction of size of the SiO_4 ring, and it is more difficult for the H_2O (or D_2O) molecule to be incorporated into the interstitial void.

5. Conclusions

SAXS, XRD and ND show that the SiO_2–13wt.% D_2O composition glass, which was synthesized by quenching from melt at 3 GPa is separated into two phases: SiO_2-rich glass phase and D_2O-rich minor phase were distributed as small domains with dimensions of less than 100 Å. Both the $S^X(Q)$ and the $S^N(Q)$ of the hydrous SiO_2 glass can be reproduced from those of the SiO_2 glass and liquid D_2O. Medium-range order and short-range order derived from XRD and ND mainly reflect the structure of the SiO_2-rich glass part. The FSDP of hydrous glass shifts to the higher-Q side than those of anhydrous glass at ambient conditions. This corresponds to the shrinkage of the medium-range order associated with the decrease of the size of SiO_4 rings by breaking the SiO_4 linkage with the OD group, as well as by distorting the network linkage of SiO_4 with a pressure of 3 GPa during glass synthesis. The response of the structure of the SiO_2-rich glass part to pressure is almost the same as that of the anhydrous SiO_2 glass. The FSDP of the hydrous glass shifts to the high-Q side with increasing pressure in parallel with that of the anhydrous glass. The Si–O–Si bond angle decreases with pressure, although the coordination number of Si is about four at the pressures of from 0.1 MPa to 10 GPa. Thus, the medium-range order shrinks with pressure associated with distortion of network linkage of SiO_4 tetrahedra. Most of D_2O molecules are in the small domains of the D_2O-rich phase and hardly penetrate into the void space in the ring consisting of SiO_4 tetrahedra of SiO_2-rich glass part.

Supplementary Materials: The following are available online at http://www.mdpi.com/2075-163X/10/1/84/s1, Figure S1: Cell assemble for the synthesis of hydrous SiO_2 glass at 3 GPa and 1873 K, Figure S2: Recovered Pt capsule and hydrous SiO_2 glass quenched from the conditions of 3 GPa and 1873 K.

Author Contributions: Conceptualization, S.U. and T.I.; formal analysis, S.U., T.H., S.K.; investigation, S.U., T.I., T.H., A.S.-F., S.K., D.W., T.S., N.F., K.-i.F.; writing—original draft preparation, S.U.; All author contribute review and editing. All authors have read and agreed to the published version of the manuscript.

Funding: This research was in part supported by the JSPS KAKENHI Grant (19GS0205, 18K03805), the Earthquake Research Institute Joint Usage/Research Program (2010-G-01, 2011-G-05, 2012-G-02), and the Joint Usage/Research Center PRIUS, Ehime University.

Acknowledgments: We thank Y. Katayama and T. Kimura for help with the ND experiments at J-PARC, and K. Mibe and M. Kanzaki for help with the synthesis of hydrous SiO_2 glass. We are grateful to A. Zeidler and P. S. Salmon for providing us with high-pressure neutron diffraction data for SiO_2 glass. We are also grateful to two anonymous reviewers for their thoughtful formal reviews. The XRD experiments were conducted under approval of PF Proposal Advisory Committee (2011G652, 2017G135) and the JASRI (2014B1480), and the ND experiments were performed with the approval of the Neutron Science Proposal Review Committee of J-PARC, MLF (2013I0011).

Conflicts of Interest: The authors declare no conflict of interest.

Appendix A

Appendix A.1 Data Reduction of X-ray and Neutron Diffraction

Appendix A.1.1 Energy Dispersive X-ray Diffraction at High Pressures

We used a Faber-Ziman definition for X-ray structure factor $S^X(Q)$ which is defined as follows.

$$S^X(Q) = (i^X_{coh}(Q) - \{\langle f(Q)^2\rangle - \langle f(Q)\rangle^2\})/\langle f(Q)\rangle^2 \quad \text{(A1)}$$

where ${i_{coh}}^{X}(Q)$ is a coherent scattering intensity per atom, $\langle f(Q)^2\rangle = \sum_i c_i f_i^2(Q)$,$\langle f(Q)\rangle^2 = (\sum_i c_i f_i(Q))^2$, c_i and $f_i(Q)$ are an atomic fraction and an atomic scattering factor of the ith atom, respectively.

The $S^X(Q)$ was evaluated by the procedure developed by Funakoshi [41]. Energy profiles of XRD pattern obtained at various Bragg angles can be expressed by the following equation.

$$I_{ob}^{X}(E,\theta) = NA(E,\theta)P(E,\theta)I_0^X(E)\left[i_{coh}^{X}(E,\theta) + i_{inc}^{X}(E,\theta) + i_m^X(E,\theta)\right] + I_{BG}^X(E,\theta) \quad \text{(A2)}$$

where N is the number of atom, $A(E,\theta)$ is the absorption factor, $P(E,\theta)$ is the polarization factor, ${I_0}^X(E)$ is the intensity of incident X-rays. ${i_{inc}}(E,\theta)^X$ and ${i_m}(E,\theta)^X$ are incoherent and multiple scattering intensity per atom, respectively. ${I_{BG}}^X(E,\theta)$ is background intensity. At first, ${I_{BG}}^X(E,\theta)$'s were subtracted from ${I_{ob}}^X(E,\theta)$'s. As the energy spectrum of incident X-rays from the synchrotron source ${I_0}^X(E)$ is unknown, we evaluated simultaneously both ${I_0}^X(E)$ and ${i_{coh}}^X(E,\theta)$'s from ${I_{ob}}^X(E,\theta)$'s by simulation using the Monte Carlo method [41]. Here, we ignored the differences of absorption and polarization effects and multiple scattering terms among data taken with different Bragg angles. The incoherent scattering term was corrected using the formulation of Hajdu [42] and Pálinkás [43]. Then coherent scattering intensities at each Bragg angle were unified to obtain ${I_{coh}}^X(Q)$. The Faber–Ziman total structure factor $S^X(Q)$ was evaluated from Equation (A1) in which the atomic scattering factor was calculated using the approximation formula given by Doyle and Turner [44].

Appendix A.1.2 Time-of-Flight Neutron Diffraction at High Pressures

Structure factor for neutron $S^N(Q)$ was evaluated from a ND profile obtained by the TOF method combined with a multi-anvil press. Observed ND profile is described as follows.

$$I_{ob}^{N}(\lambda,\theta) = NA(\lambda,\theta)I_0^N(\lambda)\left[i_{coh}^{N}(\lambda,\theta) + i_{inc}^{N}(\lambda,\theta) + i_m^N(\lambda,\theta)\right] + I_{BG}^N(\lambda,\theta) \quad \text{(A3)}$$

where N is the number of atoms, $A(\lambda,\theta)$ is the absorption factor, ${I_0}^N(\lambda)$ is the intensity of incident neutron, ${i_{coh}}^N(\lambda,\theta)$, ${i_{inc}}^N(\lambda,\theta)$, and ${i_m}^N(\lambda,\theta)$ are coherent, inelastic, incoherent, and multiple scattering cross section per one atom, respectively. ${I_{BG}}^N(\lambda,\theta)$ is background intensity. Observed scattering intensities ${I_{ob}}^N(\lambda,\theta)$ are normalized by ${I_0}^N(\lambda)$ obtained from the scattering intensity of a vanadium pellet after background subtraction and absorption correction. Absorption correction was performed according to the method of Paalman and Pings [45]. Then, incoherent scattering and multiple scattering terms were corrected. The incoherent term was evaluated by a composition average of incoherent scattering length b_{inc} of the elements, which are listed in the table of Sears [46]. The incoherent scattering for D atom was significantly deviated from the value listed in the table due to the inelastic effect. Therefore, we corrected it by empirical method employed by Kameda et al. [47] (as described below). The multiple scattering term was corrected by the method of Blech and Averbach [48]. Thus, we calculated the structure factor $S^N(Q)$ from the corrected intensity ${I_{cor}}^N(\lambda,\theta)$, which is the sum of ${i_{coh}}^N(\lambda,\theta)$ and ${i_{ine}}^N(\lambda,\theta)$.

Inelastic effect for incoherent scattering of deuterium has a small but non-negligible effect on the total scattering intensity of the hydrous SiO_2 glass. The effect was corrected based on the empirical method by Kameda et al. [48] in which incoherent scattering was estimated from the self term of the liquid null-H_2O using a known O–O correlation. The applicability of this method at PLANET has been confirmed from the good coincidence of the $S(Q)$ for D_2O water with that reported so far in the literature (Hattori et al., private com).

Definition of Faber–Ziman total structure factor for the $S^N(Q)$ is as follows.

$$S^N(Q) = (i_{coh}^N(Q) - \{\langle b\rangle^2 - \langle b\rangle^2\})/\langle b\rangle^2 \quad \text{(A4)}$$

where $\langle b^2\rangle = \sum_i c_i b_i^2$, $\langle b\rangle^2 = (\sum_i c_i b_i)^2$, c_i, and b_i are an atomic fraction and a coherent scattering length of the ith atom [46], respectively.

Appendix A.1.3 Fourier Analysis

The $S(Q)$ data in reciprocal space can be transformed into total correlation function $T(r)$ in real space by means of a Fourier transform.

$$T(r) = 4\pi r\rho_0 + \frac{2}{\pi}\int_{Q_{min}}^{Q_{max}} M(Q)Q\{S(Q)-1\}\sin rQdQ \tag{A5}$$

where ρ_0 is a number density of atoms and $M(Q)$ is a modification function. We used a Lorch function as $M(Q)$ [49].

Appendix B

Faber–Ziman Structure Factor of a Two-Phase Mixture can be Written as Follows for X-ray

$$\begin{array}{c} S^{X}_{A+B}(Q) = X_A(\langle f(Q)\rangle^2_A/\langle f(Q)\rangle^2_{A+B})S^{X}_{A}(Q) + X_B(\langle f(Q)\rangle^2_B/\langle f(Q)\rangle^2_{A+B})S^{X}_{B}(Q) \\ +X_A(\langle f(Q)^2\rangle_A - \langle f(Q)\rangle^2_A)/\langle f(Q)\rangle^2_{A+B} + X_B(\langle f(Q)^2\rangle_B - \langle f(Q)\rangle^2_B)/\langle f(Q)\rangle^2_{A+B} \\ -(\langle f(Q)^2\rangle_{A+B} - \langle f(Q)\rangle^2_{A+B})/\langle f(Q)\rangle^2_{A+B} \end{array} \tag{A6}$$

where X_A and X_B are the mole fraction of phase A and B, respectively. Here, each value satisfies the condition of $X_A + X_B = 1$. Equation (A6) can be applied to the neutron structure factor $S^{N}(Q)$ by replacing an atomic scattering factor with a coherent scattering length of neutron.

References

1. Bridgman, P.W. Effects of very high pressures on glass. *J. Appl. Phys.* **1953**, *24*, 405–413. [CrossRef]
2. Hemley, R.J.; Mao, H.K.; Bell, P.M.; Mysen, B.O. Raman spectroscopy of SiO_2 glass at high pressure. *Phys. Rev. Lett.* **1986**, *57*, 747–750. [CrossRef] [PubMed]
3. Meade, C.; Hemley, R.J.; Mao, H.K. High-pressure X-ray diffraction of SiO_2 glass. *Pys. Rev. Lett.* **1992**, *69*, 1387–1390. [CrossRef] [PubMed]
4. Inamura, Y.; Katayama, Y.; Ustumi, W.; Funakoshi, K. Transformations in the intermediate-range structure of SiO_2 glass under high pressure and temperature. *Phys. Rev. Lett.* **2004**, *93*, 015501. [CrossRef]
5. Sato, T.; Funamori, N. Sixfold-coordinated amorphous polymorph of SiO_2 under high pressure. *Phy. Rev. Lett.* **2008**, *101*, 255502. [CrossRef]
6. Benmore, C.J.; Soignard, E.; Amin, S.A.; Guthrie, M.; Shastri, S.D.; Lee, P.L.; Yarger, J.L. Structural and topological changes in silica glass at pressure. *Phys. Rev. B* **2010**, *81*, 054105. [CrossRef]
7. Sato, T.; Funamori, N. High-pressure structural transformation of SiO_2 glass up to 100 GPa. *Phys. Rev. B* **2010**, *82*, 184102. [CrossRef]
8. Wakabayashi, D.; Funamori, N.; Sato, T.; Taniguchi, T. Compression behavior of densified SiO_2 glass. *Phys. Rev. B* **2011**, *84*, 144103. [CrossRef]
9. Zeidler, A.; Wezka, K.; Rowlands, R.F.; Whittaker, D.A.J.; Salmon, P.S.; Polidori, A.; Drewitt, J.W.E.; Klotz, S.; Fischer, H.E.; Wilding, M.C.; et al. High-pressure transformation of SiO_2 glass from a tetrahedral to an octahedral network: A joint approach using neutron diffraction and molecular dynamics. *Phys. Rev. Lett.* **2014**, *113*, 13501. [CrossRef]
10. Stolper, E. Water in silicate glasses: An infrared spectroscopic study. *Contrib. Mineral. Petrol.* **1982**, *81*, 1–17. [CrossRef]
11. Tomozawa, M. Water in glass. *J. Non-Cryst. Solids* **1985**, *73*, 197–204. [CrossRef]
12. Zotov, N.; Keppler, H.; Hannon, A.C.; Soper, A.K. The effect of water on the structure of silicate glasses—A neutron diffraction study. *J. Non-Cryst. Solids* **1996**, *202*, 153–163. [CrossRef]
13. Van der Steen, G.H.A.M.; van den Boom, H. Raman spectroscopic study of hydrogen-containing vitreous silica. *J. Non-Cryst. Solids* **1977**, *23*, 279–286. [CrossRef]
14. McMillan, P.F.; Remmele, R.L. Hydroxyl sites in SiO_2 glass: A note on infrared and Raman spectra. *Am. Mineral.* **1986**, *71*, 772–778.

15. Sato, T.; Funamori, N.; Wakabayashi, D.; Nishida, K.; Kikegawa, T. Coexistence of two states in optically homogeneous silica glass during the transformation in short-range order. *Phys. Rev. B* **2018**, *98*, 144111. [CrossRef]
16. Kohara, S.; Suzuya, K.; Kashihara, K.; Matsumoto, N.; Umesaki, N.; Sakai, I. A horizontal two-axis diffractometer for high-energy X-ray diffraction using synchrotron radiation on bending magnet beamline BL04B2 at SPring-8. *Nucl. Instrum. Methods Phys. Res.* **2001**, *A467–A468*, 1030–1033. [CrossRef]
17. Kohara, S.; Suzuya, K. High-energy X-ray diffraction studies of disordered materials. *Nucl. Instrum. Methods Phys. Res.* **2003**, *B199*, 23–28. [CrossRef]
18. Decker, D.L. High-pressure equation of state for NaCl, KCl, and CsCl. *J. Appl. Phys.* **1971**, *42*, 3239–3244. [CrossRef]
19. Sano-Furukawa, A.; Hattori, T.; Arima, H.; Yamada, A.; Tabata, S.; Kondo, M.; Nakamura, A.; Kagi, H.; Yagi, T. Six-axis multi-anvil press for high-pressure, high-temperature neutron diffraction experiments. *Rev. Sci. Instrum.* **2014**, *85*, 113905. [CrossRef]
20. Hattori, T.; Sano-Furukawa, A.; Arima, H.; Komatsu, K.; Yamada, A.; Inamura, Y.; Nakatani, T.; Seto, Y.; Nagai, T.; Utsumi, W.; et al. Design and performance of high-pressure PLANET beamline at pulsed neutron source at J-PARC. *Nucl. Instrum. Methods Phys. Res.* **2015**, *A780*, 55–67. [CrossRef]
21. Nishiyama, N.; Wang, Y.; Sanehira, T.; Irifune, T.; Rivers, M.L. Development of the multi-anvil assembly 6-6 for DIA and D-DIA type high-pressure apparatuses. *High Press. Res.* **2008**, *28*, 307–314. [CrossRef]
22. Kohara, S.; Ito, M.; Suzuya, K.; Inamura, Y.; Sakurai, Y.; Ohishi, Y.; Takata, M. Structural studies of disordered materials using high-energy X-ray diffraction from ambient to extreme conditions. *J. Phys. Condens. Matter* **2007**, *19*, 506101. [CrossRef]
23. Hannon, A.C. Unpublished GEM Datra Examples: Silica Glass, Diffraction Data for Vitreous SiO_2, Oxide Glass Data. 1990. Available online: https://www.isis.stfc.ac.uk/Pages/Oxide-Glass-Data.aspx (accessed on 3 December 2019).
24. Kameda, Y.; Amo, Y.; Usui, T.; Umebayashi, Y.; Ikeda, K.; Otomo, T. Neutron diffraction study on partial pair correlation functions of water at ambient temperature. *Bull. Chem. Soc. Jpn.* **2018**, *91*, 1586–1595. [CrossRef]
25. Elliot, S.R. Medium-range structural order in covalent amorphous solids. *Nature* **1991**, *354*, 445–452. [CrossRef]
26. Gaskell, P.H. Medium-range structure in glasses and low-Q structure in neutron and X-ray scattering data. *J. Non-Cryst. Solids* **2005**, *351*, 1003–1013. [CrossRef]
27. Crupi, C.; Carini, G.; González, M.; D'Angelo, G. Origin of the first sharp diffraction peak in glasses. *Phys. Rev. B* **2015**, *92*, 134206. [CrossRef]
28. Zeidler, A.; Salmon, P.S. Pressure-driven transformation of the ordering in amorphous network-forming materials. *Phys. Rev. B* **2016**, *93*, 214204. [CrossRef]
29. Onodera, Y.; Kohara, S.; Tahara, S.; Masuno, A.; Inoue, H.; Shiga, M.; Hirata, A.; Tsuchiya, K.; Hiraoka, Y.; Obayashi, I.; et al. Understanding diffraction patterns of glassy, liquid and amorphous materials via persistent homology analyses. *J. Ceram. Soc. Jpn.* **2019**, *127*, 853–863. [CrossRef]
30. Pasquarello, A.; Car, R. Identification of Raman defect lines as signatures of ring structures in vitreous silica. *Phys. Rev. Lett.* **1998**, *80*, 5145–5147. [CrossRef]
31. Zotov, N.; Yanev, Y.; Epelbaum, M.; Konstantinov, L. Effect of water on the structure of rhyolite glasses—X-ray diffraction and Raman spectroscopy studies. *J. Non-Cryst. Solids* **1992**, *142*, 234–246. [CrossRef]
32. Susman, S.; Volin, K.J.; Price, D.L.; Grimsditch, M.; Rino, J.P.; Kalia, R.K.; Vashishta, P.; Gwanmessia, G.; Wang, Y.; Libermann, R.C. Intermediate-range order in permanently densified vitreous SiO_2: A neutron-diffraction and molecular-dynamics study. *Phys. Rev. B* **1991**, *43*, 1994–1997. [CrossRef] [PubMed]
33. Onodera, Y.; Takimoto, Y.; Hijiya, H.; Taniguchi, T.; Urata, S.; Inaba, S.; Fujita, S.; Obayashi, I.; Hiraoka, Y.; Kohara, S. Origin of the mixed alkali effect in silicate glass. *NPG Asia Mater.* **2019**, *11*, 75. [CrossRef]
34. Hart, R.T.; Benmore, C.J.; Neuefeind, J.; Kohara, S.; Tomberli, B.; Egelstaff, P.A. Temperature dependence of isotropic quantum effects in water. *Phys. Rev. Lett.* **2005**, *94*, 047801. [CrossRef] [PubMed]
35. Kameda, Y.; Uemura, O. The intramolecular structure of oxonium ion in concentrated aqueous deuterochloric acid solutions. *Bull. Chem. Soc. Jpn.* **1992**, *65*, 2021–2028. [CrossRef]
36. Funamori, N.; Sato, T. A cubic boron nitride gasket for diamond-anvil experiments. *Rev. Sci. Instrum.* **2008**, *79*, 053903. [CrossRef]
37. Sakamaki, T. Density of hydrous magma. *Chem. Geol.* **2017**, *475*, 135–139. [CrossRef]

38. Sato, T.; Funamori, N.; Yagi, T. Helium penetrates into silica glass and reduces its compressibility. *Nat. Commun.* **2011**, *2*, 345. [CrossRef]
39. Shacckelford, J.F.; Masaryk, J.S. The interstitial structure of vitreous silica. *J. Non-Cryst. Solids* **1978**, *30*, 127–139. [CrossRef]
40. Zhang, Y.; Xu, Z. Atomic radii of noble gas elements in condensed phases. *Am. Mineral.* **1995**, *80*, 670–675. [CrossRef]
41. Funakoshi, K. Energy-dispersive X-ray Diffraction Study for Alkali Silicate Melts Using Synchrotron Radiation under High Pressure and Temperature. Ph.D. Thesis, Tokyo Institute of Technology, Tokyo, Japan, March 1997.
42. Hajdu, F. Analytic approximation for incoherent scattering X-ray intensities. *Acta Crystallogr.* **1971**, *A27*, 73–74. [CrossRef]
43. Pálinkás, G. Analytic approximation for the incoherent X-ray intensities of the atoms from Ca to Am. *Acta Crystallogr.* **1973**, *A29*, 10–12. [CrossRef]
44. Doyle, P.A.; Turner, P.S. Relativistic Hartree-Fock X-ray and electron scattering factors. *Acta Crystallogr.* **1968**, *A24*, 390–397. [CrossRef]
45. Paalman, H.H.; Pings, C.J. Numerical evaluation of X-ray absorption Factors for cylindrical samples and annular sample cells. *J. App. Phys.* **1962**, *33*, 2635–2639. [CrossRef]
46. Sears, V.F. Neutron scattering lengths and cross sections. *Neutron News* **1992**, *3*, 26–37. [CrossRef]
47. Kameda, Y.; Sasaki, M.; Usuki, T.; Otomo, T.; Itoh, K.; Suzuya, K.; Fukunaga, T. Inelasticity effect on neutron scattering intensities of the null-H_2O. *J. Neutron Res.* **2003**, *11*, 153–163. [CrossRef]
48. Blech, I.A.; Averbach, B.L. Multiple scattering of neutrons in vanadium and copper. *Phys. Rev.* **1965**, *137*, A113–A116. [CrossRef]
49. Lorch, E. Neutron diffraction by germania, silica and radiation-damaged silica glasses. *J. Phys. C Solid State Phys.* **1969**, *2*, 229–237. [CrossRef]